

---

# Comparing Two Climatologies of the Labrador Sea: Geopotential and Isopycnal

Nilgun Kulan<sup>†</sup> and Paul G. Myers\*

*Department Earth and Atmospheric Sciences  
University of Alberta, Edmonton AB T6G 2E3*

[Original manuscript received 1 September 2006; accepted 2 July 2008]

---

**ABSTRACT** Two climatologies, one using an isopycnal approach and the other employing a more classical geopotential approach, are produced for the Labrador Sea region. These differ from existing climatologies through the use of smaller search radii, more data and a carefully chosen depth dependent correction scheme. This results in the preservation of the strong fronts that exist between cold, fresh boundary currents and warmer, more saline interior waters and, in general, less smoothing of features. The waters of the West Greenland Current, the Labrador Current and the interior are well represented, especially Labrador Sea Water and the Deep Western Boundary Current. We consider that our 'best' results are produced by the isopycnal climatology. Isopycnal averaging gives more realistic results by reducing artificial mixing of water properties and preserving the baroclinicity of the flow.

We estimate the total transport, using the results from the isopycnal climatology in a diagnostic model driven by climatological winds. For the Labrador Current/subpolar gyre at 53°N we find a transport of 46.6 Sv southward, with 9.7 Sv of that being Labrador Sea Water, 12.1 Sv being Gibbs Fracture Zone Water and 8.0 Sv being Denmark Strait Overflow Water. Transport into the Labrador Sea is 41.2 Sv with 6.6 Sv of Labrador Sea Water exported back to the Irminger Sea. Total southward freshwater transport by the Labrador Current (including slope and 'gyre' branches) is 239 mSv at 53°N, with almost 60% of this carried in the upper layer. Import of fresh water to the Labrador Sea from the east in the East Greenland Current is 129 mSv, which is divided almost equally among all layers. Our estimate of the long-term mean formation rate of Labrador Sea Water is between 3.6 and 3.8 Sv.

**RÉSUMÉ** [Traduit par la rédaction] Nous produisons deux climatologies, l'une utilisant une approche isopycne et l'autre une approche géopotentielle plus classique, pour la région de la mer du Labrador. Ces climatologies diffèrent des climatologies existantes par l'emploi de plus petits rayons d'exploration, de plus de données et d'un schéma de correction lié à la profondeur soigneusement choisi. Cela a pour effet de préserver les fronts nets qui existent entre les courants de bord froids et doux et les eaux de l'intérieur chaudes et plus salées et, en général, de produire moins de lissage des caractéristiques. Les eaux du courant groenlandais de l'Ouest, du courant du Labrador et de l'intérieur sont bien représentées, surtout les eaux de la mer du Labrador et le courant profond de bord ouest. Nous considérons que nos « meilleurs » résultats proviennent de la climatologie isopycne. Le moyennage isopycne donne des résultats plus réalistes en réduisant le mélange artificiel des propriétés de l'eau et en préservant la baroclinité de l'écoulement.

Nous estimons le transport total en utilisant les résultats de la climatologie isopycne dans un modèle diagnostique piloté par les vents climatologiques. Pour le courant du Labrador/circulation subpolaire à 53°N, nous trouvons un transport de 46,6 Sv vers le sud, dont 9,7 Sv sont des eaux de la mer du Labrador, 12,1 Sv sont des eaux de la zone de fracture Gibbs et 8,0 Sv sont des eaux de débordement du détroit du Danemark. Le transport entrant dans la mer du Labrador est de 41,2 Sv, avec 6,6 Sv des eaux de la mer du Labrador retournées dans la mer Irminger. Le transport total d'eau douce vers le sud par le courant du Labrador (y compris les sections de la pente et de la « circulation ») est de 239 mSv à 53°N, dont presque 60 % sont transportés dans la couche supérieure. L'importation d'eau douce vers la mer du Labrador par l'est dans le courant groenlandais de l'est est de 129 mSv, qui se divisent presque également dans toutes les couches. Notre estimation du taux de formation moyen à long terme d'eau de la mer du Labrador est entre 3,6 et 3,8 Sv.

---

## 1 Introduction

The Labrador Sea (Fig. 1) is located at the northern extremity of the Atlantic Ocean, roughly between Newfoundland and Labrador to the west and Greenland to the east. It is connect-

ed to the Arctic Ocean through Baffin Bay to the north and open to the Atlantic Ocean to the south. The basin-scale circulation pattern in the Labrador Sea is cyclonic, part of the

---

\*Corresponding author's e-mail: [pmyers@ualberta.ca](mailto:pmyers@ualberta.ca)

<sup>†</sup>Current affiliation: Institute of Ocean Sciences, Fisheries and Oceans Canada, Victoria BC

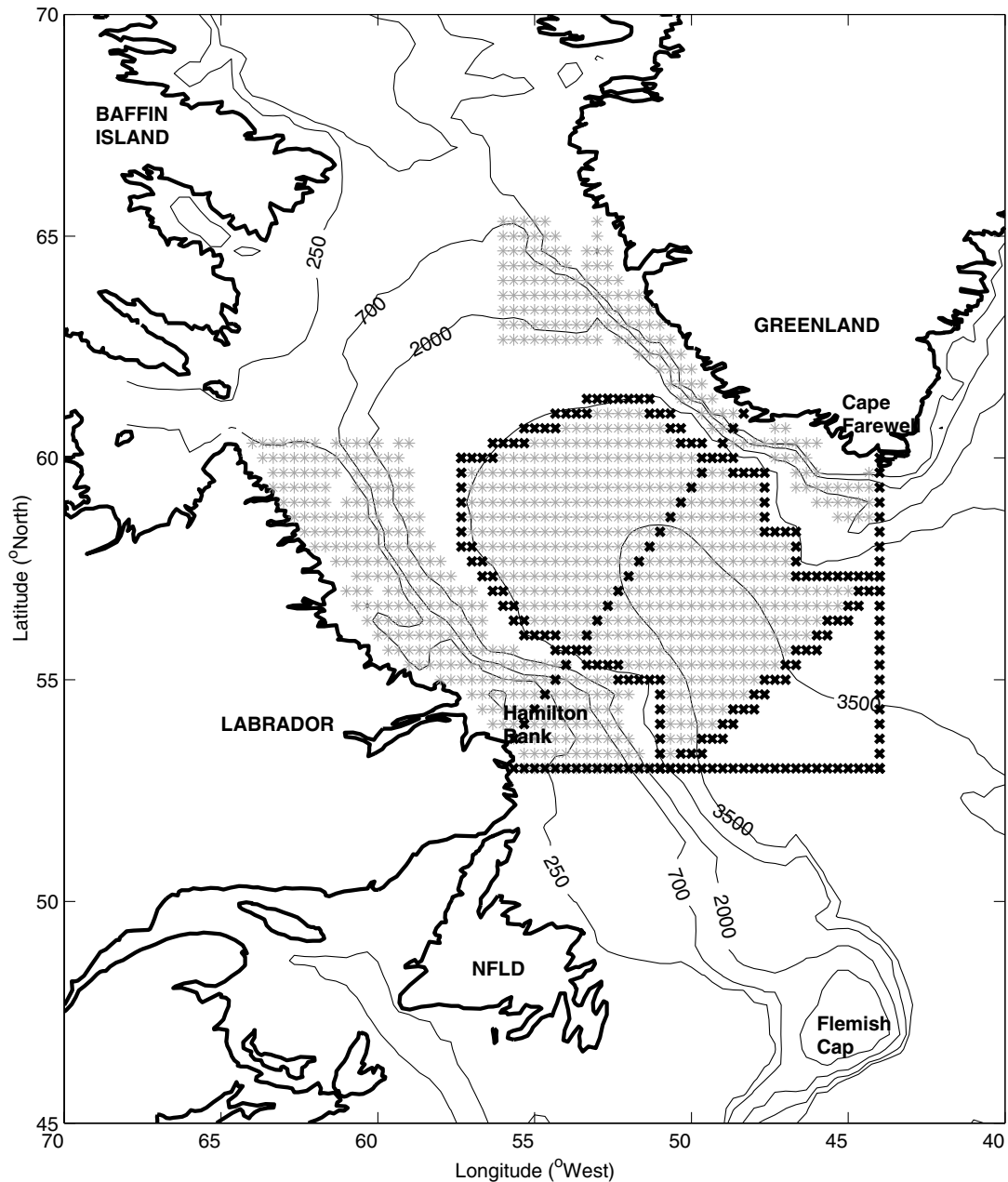


Fig. 1 A map of the study region, showing the three areas we focus on: the West Greenland Current, the Labrador Current and the interior. The map also shows the cross-Labrador Sea and the 53°N and the 44°W sections for which we present results.

subpolar gyre. At the surface, cold and fresh boundary currents flow as narrow jets concentrated over the steepest topography, with relatively large current velocities (approximately  $30 \text{ cm s}^{-1}$ ; Flatau et al. (2003). On the Greenland side, a northwestward flowing boundary current known as the West Greenland Current (WGC) brings low salinity ( $<34.5$ ) near-freezing ( $-1.8^\circ\text{C}$ ) waters of Arctic origin to the Labrador Sea around the tip of Cape Farewell (Clarke, 1984) offshore of which flows the warm and more saline Irminger water (IW; Cuny et al., 2002). Over the wider continental shelf and shelf break off Labrador, lies the southeastward flowing Labrador Current (LC). Furthermore, Lazier and Wright (1993) report-

ed a second branch of the LC, concentrated over the 2500 m isobath, offshore of the 'classical' LC, and named it the 'deep' LC, accordingly. The deep LC has a strong barotropic component, while the classical LC is primarily baroclinic. The deep LC is considered to be part of the large-scale subpolar gyre circulation (Thompson et al., 1986), which is stronger in winter and weaker in summer (Greatbatch and Goulding, 1989). Offshore, evidence of recirculation has been revealed by float analysis (Lavender et al., 2002).

At depth, the Labrador Sea circulation is still cyclonic and acts as a pathway for the various components of the Deep Western Boundary Current (DWBC). The deepest part of the

central Labrador Sea is filled with the convective product of the Nordic Seas, known as the Denmark Strait Overflow Water (DSOW). DSOW is slightly fresher than the overlying water mass, but its low temperature ( $T = 0.8^\circ$  to  $1.5^\circ\text{C}$ ,  $S$  approximately 34.9,  $\sigma_\theta > 28.88$ ) makes this water mass the most dense of all North Atlantic water masses.

Above the DSOW, lies the Northeast Atlantic Deep Water (NEADW), which originates in the Nordic Seas and the northeastern Atlantic ( $T$  approximately  $3^\circ\text{C}$ ,  $S$  approximately 34.95,  $28.80 > \sigma_\theta > 28.88$ ). In recent literature, this water mass is referred to as the Gibbs Fracture Zone Water (GFZW) (e.g., Smethie and Swift, 1989). Both the DSOW and GFZW move cyclonically around the Labrador Sea and leave the basin east of Flemish Cap (Fischer et al., 2004). The Labrador Sea Water (LSW) lies above the two deep components of the Deep Western Boundary Current (DWBC), the GFZW and DSOW, and below the warmer, more saline IW (Fischer et al., 2004). Fischer et al. (2004) define LSW as the water mass with a density between  $\sigma_\theta = 27.74$  and  $\sigma_\theta = 27.80$ . The  $T$  and  $S$  values of LSW are known to exhibit interannual and interdecadal variability (Yashayaev, 2007).

The interior waters of the Labrador Sea are warmer and more saline than the boundary currents. Weak stratification keeps the basin ice free as the surface layer cannot be sufficiently cooled to the freezing point without convective overturning. Lateral fluxes of heat and salt from the northwest corner of the North Atlantic Current (NAC:  $T$  approximately  $9.5^\circ\text{C}$  and  $S$  approximately 35.35 (Clarke, 1984)), and from the IW ( $T$  approximately  $4.5^\circ\text{C}$  and  $S$  approximately 34.95 (Cuny et al., 2002)) help restratify the basin after convection (Lilly et al., 1999; Straneo, 2006). Thus, intensified air-sea heat fluxes in winter can cause enough buoyancy loss to produce the LSW, a mid-depth water mass, via convective overturning. This newly formed water mass lies roughly between 500 and 1500 m of the water column. However, it should be noted that the production rate of LSW (as estimated from the maximum depth the convective overturning reaches in a particular year) is found to vary significantly with time (Lazier et al., 2002; Lilly et al., 1999; Pickart et al., 2002).

In addition to the seasonal variability, which is the fundamental mode of variability, interannual and quasi-decadal oscillations in the formation, spreading and physical properties of LSW and other water masses have been identified (e.g., Dickson et al., 2002). Therefore, the snapshot descriptions of temperature, salinity and currents obtained from direct observations (e.g., Lazier, 1973; Clarke and Gascard, 1983; Lazier and Wright, 1993; Pickart et al., 2002), which are irregularly distributed over time and space cannot represent the mean state of the Labrador Sea. On the other hand, an ocean climatology is assembled by taking an average of observed quantities over a number of years, in which case transient features are filtered out during the averaging process and replaced by persistent flow features. In a region where the variability is so high, such as the Labrador Sea, one can ask whether a climatology can ever represent the actual hydrography of the region. Since, to understand the variability in a

region, one must have some idea of the mean state around which the system is changing, there is a need for climatologies. Such products can provide a benchmark for interpreting observational data and model results and provide an assessment of variability. Additionally, such averaged fields are of use for the initialization and/or validation of numerical models. Therefore this work focuses on two climatologies for the Labrador Sea.

The Levitus (1982, 1994), Reynaud et al. (1995), de Young et al. (1994), Lozier et al. (1995), Grey et al. (1999) and Yashayaev and Zveryaev (2001) climatologies are several examples of climatologies that include the Labrador Sea (Table 1). Some of these climatologies were produced for the global ocean while others focused on a particular basin. Climatologies built for the world ocean (e.g., Levitus, 1982, 1994) are generally of coarser resolution to account for the large data-sparse regions in the Southern Ocean. Although the Lozier et al. (1995) climatology for the North Atlantic had the same horizontal resolution as the global climatologies, the focus on one basin allowed a smaller smoothing scale and thus the effective resolution was increased. de Young et al. (1994) used a very fine resolution ( $1/12^\circ \times 1/12^\circ$ ) for their regional climatology. However, using such a high resolution produces unfilled grid points in the northern latitudes where the data coverage is limited, especially in winter.

We thus chose to use a resolution of  $1/3$  of a degree, as did Reynaud et al. (1995) whose climatology might be the closest to ours with respect to the choice of domain, resolution and objective analysis scheme. The biggest difference between the geopotential climatology produced as the first part of this study and the work of Reynaud et al. (1995) is the large amount of additional data that have become available over the last decade permitting the use of smaller search radii. The increased number of measurements taken in the Labrador Sea in the 1990s as a result of regional and global programs, such as the Labrador Sea Experiment and the World Ocean Circulation Experiment, has supplemented the hydrographic database and has provided additional motivation to carry out this study. The details of the data coverage and quality control procedures can be found in the next two sections.

Spatial smoothing is introduced when unevenly distributed observations are mapped onto regular grid points in the horizontal and vertical. However, the degree of smoothing can be kept to a minimum by applying an appropriate objective analysis technique. Traditionally, the data are first binned in the vertical, according to either their depth (geopotential coordinates) or potential density (isopycnal coordinates) range. Isopycnal coordinates provide a more natural system since water tends

to mix along isopycnals rather than along isobaths. The advantages of using isopycnal coordinates over geopotential coordinates are discussed in detail in Lozier et al. (1995). Isopycnal coordinates have been widely used in climatological studies of the world oceans (Grey et al., 1999; Lozier et al., 1995). This favours isopycnal mixing over diapycnal mixing, thus avoiding artificial mixing of water properties;

TABLE 1. Summary of the climatologies referred to in the introduction for comparison with those presented in this paper.

Climatology	Domain	Vertical Coordinate	Resolution	Smallest Smoothing
Levitus (1982)	Global	Geopotential	1 degree	772 km
Reynaud et al. (1995)	Labrador Sea	Geopotential	1/4 degree	200 km
de Young et al. (1994)	Labrador Sea	Geopotential	1/12 degree	–
Lozier et al. (1995)	N. Atlantic	Isopycnal	1 degree	100–300 km
Boyer et al. (2005)	Global	Geopotential	1/4 degree	214 km
Yashayaev and Zveryaev (2001)	Basin	Sea Surface Temperature	2 degrees	–

although it must be noted that isobaric mapping could produce a similar field if the radius of correlation is small enough and compatible with the data distribution. Furthermore, isopycnal averaging preserves baroclinicity of the flow field, which we will highlight in our results, especially with respect to the DWBC.

Section 2 presents the data used, the quality control carried out on the data and the methodology used to produce the climatological data sets presented here. We then present the climatological results, comparing them with observations to show that our results produce a realistic representation of the hydrography of the Labrador Sea. We also compare and contrast the geopotential and isopycnal climatologies with each other, as well as with existing climatologies. Finally, we examine the mean large-scale water properties of the Labrador Sea on annual and seasonal time scales, as well as the transports.

## 2 Data

### a Area of Interest, Data Source and Distribution

All the temperature and salinity data used in this study were extracted from an extensive hydrographic database maintained by the Bedford Institute of Oceanography (BIO; Gregory, 2004). The Climate Database<sup>a</sup> incorporates temperature and salinity data collected using various instruments including hydrographic bottles, Conductivity-Temperature-Depth instruments (CTDs), batfish tows, and bathythermographs. After the initial quality controls applied by the original institute or organization, the data are validated by the Marine Environmental Data Service (MEDS) according to the procedures described in the Intergovernmental Oceanographic Commission (IOC) publication – Manuals and Guides 22: GTSP real-time quality control manual<sup>b</sup>. The additional quality control procedures include location and identification tests, density inversion tests for profile data, climatological tests against known climatologies and visual inspection of the data. We carry out an additional basic range check using  $-1.8^{\circ}$  to  $25^{\circ}\text{C}$  for temperature and 10 to 37 for salinity, which removed only 1731 individual observations.

<sup>a</sup>Details on the contents of the database and how to access the data through a query system can be obtained at

<http://www.mar.dfo-mpo.gc.ca/science/ocean/database/climapp.html>.

<sup>b</sup>A copy of this manual can be obtained at

<http://www.nodc.noaa.gov/GTSP/document/qcmans/mg22/guide22.htm>.

For this study, only observations for years up to and including 2000 with both temperature and salinity measurements collected over an area bounded by  $40^{\circ}$  to  $70^{\circ}\text{W}$  longitude and  $45^{\circ}$  to  $70^{\circ}\text{N}$  latitude and populated in the database prior to April 2002 were extracted from the climate database. Data densities for the surface and the 27.74–27.80 isopycnal layer are shown in Fig. 2. Topographic data are extracted from the National Geophysical Data Center's 5-minute resolution ocean floor dataset (NOAA, 1988) and interpolated onto a  $1/3^{\circ} \times 1/3^{\circ}$  grid for the Labrador Sea region.

Besides a long-term trend in the data availability (Fig. 3b), a bias towards the warmer months of the year is also evident (Fig. 3b). Apart from the temporal bias, the data contain spatial biases. For example, Ocean Weather Station Bravo (OWS-Bravo), which was located at about  $56^{\circ}30'\text{N}$ ,  $51^{\circ}00'\text{W}$ , provided oceanographic data between 1964 and 1974 with unparalleled temporal resolution. The high density of observations at this location, as well as at some other frequently visited stations and transect lines, can easily be seen in Fig. 2a.

An earlier version of the climatology was compiled without down-sampling the data from OWS-Bravo. The results were severely biased to the low salinity climatic conditions present during the tenure of OWS-Bravo, especially in the deep Labrador Sea (approximately 1000 m) as the number of observations made in the deep, central Labrador Sea during the OWS-Bravo era greatly outnumbers any other period. The down-sampling is implemented to include approximately one OWS-Bravo datum per season over a particular depth or isopycnal layer. This is achieved by randomly including only 1 out of every 100 original observations from OWS-Bravo in our analysis. The selection of the data points was independent in each layer.

We next bin the data in the vertical using two approaches, geopotential (or isobaric) and isopycnal. No interpolation was performed, and each data point was assigned to the appropriate layer. If a profile did not have a data point within a given layer, no value was assigned. Throughout the rest of this section, the analysis procedures we discuss were applied to each and every geopotential and isopycnal layer equally.

The data were sorted into 12 groups according to the month (January – December) in which they were collected. Then, they were binned geographically into  $5^{\circ} \times 5^{\circ}$  squares in the northern part of the domain (between  $60^{\circ}\text{N}$  and  $70^{\circ}\text{N}$ ), where the data density is low, and into  $2.5^{\circ} \times 2.5^{\circ}$  squares in the southern part of the domain (between  $45^{\circ}\text{N}$  and  $60^{\circ}\text{N}$ ). At this

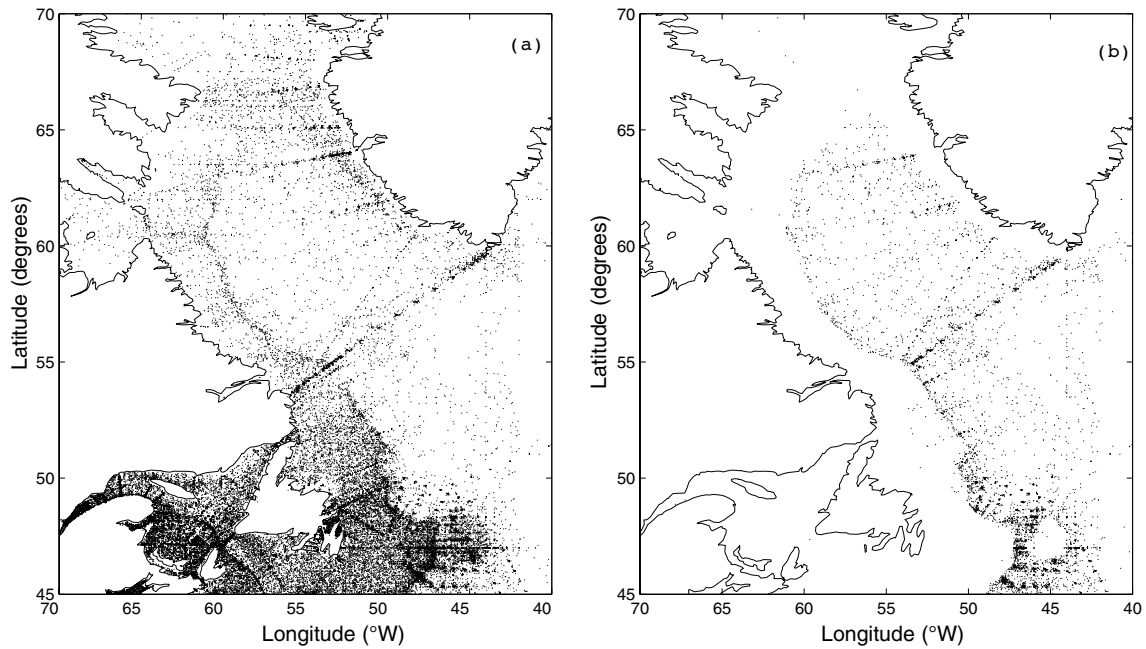


Fig. 2 Original data density distribution on a particular layer used for the calculation of GEO and ISO climatologies. The layers shown here are (a) the surface layer ( $z = 0$  to 5 db) of the geopotential and (b) the LSW density layer ( $\sigma_{\theta} = 27.74$  to 27.80) of the isopycnal climatology. Every dot represents an observation made at the location.

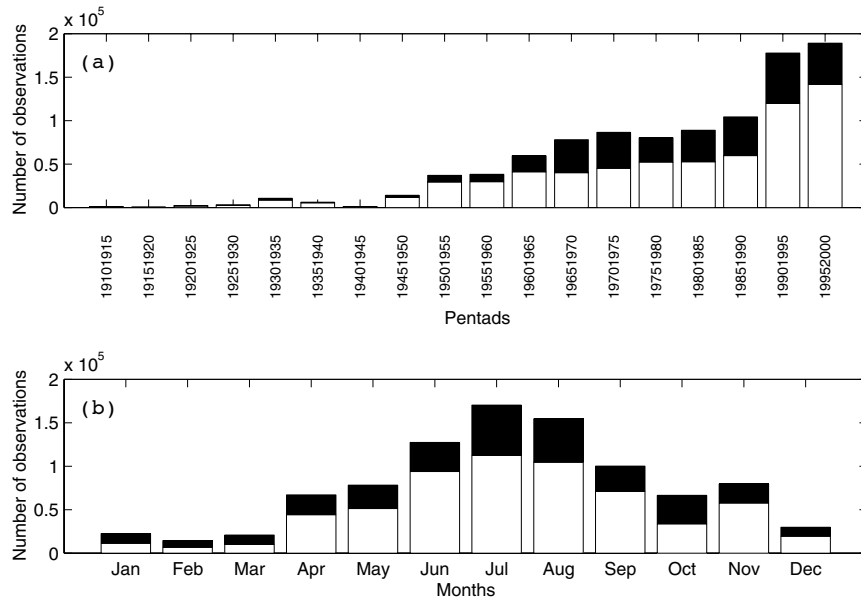


Fig. 3 Total number of observations over a) pentads and b) months of the year. Dark shading represents the portion of the data rejected according to the statistical and bias removal procedures.

point, binned data were examined to determine whether a single cruise contributed more than one-fifth of all the observations in a predetermined bin (i.e., within a geographical box and between each layer). In that case, all but three data values from this cruise were rejected (randomly and independently for each layer) before turning on the outlier removal procedures in order to avoid biased statistical means and standard deviations. Although 20% is an ad hoc criterion, we felt a

consistent approach was needed that could be used in data sparse areas as well as more densely sampled areas. The binned data were subjected to a  $\pm 3$  standard deviation ( $\sigma$ ) criterion in such a way that if a property value deviated more than three standard deviations around the mean calculated for a particular square and month, it was rejected. A  $\pm 3\sigma$  criterion is more stringent than that used in some other climatological studies (e.g., MacDonald et al., 2001). The choice of a

narrower window in our case was justified due to the shorter time scale over which the data were binned (i.e., one month).

After this preliminary statistical clean up, another statistical check with varying spatial and temporal scales was applied. For this analysis the data were grouped into four seasons: winter (January, February, March), spring (April, May, June), summer (July, August, September), and fall (October, November, December). Then seasonal and annual means and standard deviations were calculated by using a search radius of 150 km, the smallest radius of influence employed in the objective analysis (OA; discussed in more detail in Section 3), at each grid point. The depth dependence factor of the objective analysis scheme was also switched on in the calculation of the mean and standard deviation at a grid point. Following the same  $\pm 3\sigma$  criterion as with the monthly check, data points that fell outside the  $\pm 3\sigma$  window around the mean were excluded.

More detail about the vertical data distribution after the quality control and bias removal for the geopotential and isopycnal layers can be found in Tables 2 and 3, respectively. The geopotential (isopycnal) (GEO (ISO)) climatology has 44 standard isobaric (density) layers in the vertical between the surface and 4600 m ( $\sigma_\theta = 17.95$  and 28.00). The total number of observations used in the compilation of the GEO climatology is 643,966 and 620,992 for the ISO climatology. The slight difference in the total number of observations between the GEO and ISO climatologies stems from the fact that the initial clean-up statistical tests (including the downscaling at OWS-Bravo) were performed on different coordinates (geopotential versus isopycnal) in the vertical. Figure 3 also shows the increased number of observations available in the 1990s through the use of CTDs with high vertical resolution. Although every attempt has been made to avoid biases (see previous), this greater vertical resolution may cause a bias to the cold, strong LSW class conditions of the 1990s especially in the deeper layers.

### 3 Methodology

#### a Method of Successive Correction (MSC)

The observations over a domain are unevenly distributed along cruise tracks, moorings and stations; however, numerical models often require the input data to be on a regular grid. The same is true for the comparison of variables and for plotting the property fields. Therefore, interpolation of data from irregularly distributed observations onto regular grids is a common procedure.

A variety of iterative schemes has been used in the North Atlantic to produce gridded property maps. These studies include:

- The application of the original iterative difference-correction objective analysis scheme in Levitus' World Ocean Atlases (Levitus, 1982, 1994)
- Iterative correction method with directionality (de Young et al., 1994)
- Iterative correction method with depth dependence (Reynaud et al., 1995)

In this study an iterative difference-correction scheme based on Cressman (1959) with depth dependence is employed. It starts by generating a first-guess field for every grid point. Then, the initial guess is corrected by the weighted mean of the differences between the guess value and all measurements within the radius of influence. The weight function ( $W_s$ ) used in this study is the one suggested by Barnes (1964). The corrected value calculated at the end of one iteration is then used as the first-guess field for the next iteration. This entire process is repeated several times, decreasing the radius of influence with each iteration. Starting with a large radius of influence and moving towards smaller radii of influence enables gaps in the property fields to be filled by assigning large-scale averages to data-deficient grids, then progressively adds small-scale details to them by decreasing the radius of influence.

A general formulation for this scheme is  $G_{i,j} = S_{guess,i,j} + C_{i,j}$  where  $G_{i,j}$  is the analyzed value,  $S_{guess,i,j}$  is the first-guess, and  $C_{i,j}$  is the correction value (weighted sum of observation increments):  $C_{i,j} = (\sum W_s Q_s) / \sum W_s$  where  $Q_s = S_{guess,i,j} - S_p$ ,  $W_s = 0$  for  $r > R$  and  $W_s = e^{-4(r/R)^2}$  for  $r \leq R$  where  $r$  is the distance between the observation,  $S_p$ , and the grid point. The initial guess,  $S_{guess}$ , is corrected by the weighted mean of the differences between that value and all measurements,  $S_p$ , within the radius of influence,  $R$ . The weight function is iteration dependent since it includes the search radius which is progressively reduced.

The iterations were repeated three times with radii of influence of 500 km, 300 km, and 150 km, respectively. The number of iterations and the radii of influence are limited by the data density and the horizontal grid resolution. The number of observations available for this study is significantly larger than those used in previous Labrador Sea climatologies, which explains the smaller radii of influence chosen here compared to the earlier studies (e.g.,  $R_1 = 892$  km,  $R_2 = 669$  km,  $R_3 = 446$  km,  $R_4 = 771$  km in Stephens et al. (2002), and  $R_1 = 800$  km,  $R_2 = 500$  km,  $R_3 = 200$  km in Reynaud et al. (1995). The specific radii were chosen as a balance between a desire to reduce smoothing and the need for a first radius large enough to ensure that gaps would be filled in the northern part of the domain, the deep ocean and during winter. Since the objective analysis scheme introduces smoothing to a certain degree, no other smoothing technique was applied between the iterations except after the last iteration.

Since horizontal gradients are much stronger across boundary currents than along them or within the interior, the assumption of isotropy consistent with a fixed radius of influence is not realistic. If this assumption is not relaxed, the mixing of different water masses leads to additional and unwanted smoothing and a poor representation of fronts and boundary currents.

Thus, taking advantage of a strong relationship between water mass distribution and bathymetry, an additional search criterion to include data only from a range of isobaths was suggested by Reynaud et al. (1995). The spatial distance  $r$  is redefined as:  $r = d + R\delta$  where  $d$  is the real spatial distance

## Comparing Two Climatologies of the Labrador Sea: Geopotential and Isopycnal / 25

TABLE 2. Standard geopotential layers, their depth range, and the number of observations that fall within each layer after bias removal and quality control checks.

Depth Level	Range (m) $\leq x <$	Number of Data Points	Depth Level	Range (m) $\leq x <$	Number of Data Points
1	0–5	70879	23	1050–1150	1415
2	5–15	54094	24	1150–1250	2196
3	15–25	54245	25	1250–1350	1031
4	25–35	57696	26	1350–1450	1172
5	35–45	28497	27	1450–1550	2092
6	45–55	54704	28	1550–1650	593
7	55–70	26758	29	1650–1750	363
8	70–90	46376	30	1750–1850	497
9	90–110	43862	31	1850–1950	416
10	110–130	21400	32	1950–2100	1260
11	130–150	20721	33	2100–2300	448
12	150–180	31512	34	2300–2500	550
13	180–220	29683	35	2500–2700	471
14	220–275	20932	36	2700–2900	359
15	275–350	20557	37	2900–3100	441
16	350–450	13859	38	3100–3300	274
17	450–550	9329	39	3300–3500	268
18	550–650	7698	40	3500–3700	180
19	650–750	3323	41	3700–3900	62
20	750–850	6103	42	3900–4125	45
21	850–950	2617	43	4125–4375	26
22	950–1050	4947	44	4375–4825	15

TABLE 3. Standard isopycnal layers, their depth ranges, and the number of observations that fall within each layer after bias removal and quality control checks.

Density Surface	Range $\leq \sigma_\theta <$	Number of Data Points	Density Surface	Range (m) $\leq \sigma_\theta <$	Number of Data Points
1	17.95–19.95	2820	23	26.89–26.98	18400
2	19.95–20.95	5376	24	26.98–27.05	16545
3	20.95–21.95	9620	25	27.05–27.12	16106
4	21.95–22.95	14107	26	27.12–27.19	16253
5	22.95–23.45	12955	27	27.19–27.26	15688
6	23.45–23.95	15668	28	27.26–27.33	15644
7	23.95–24.45	18554	29	27.33–27.40	15127
8	24.45–24.75	17230	30	27.40–27.45	12601
9	24.75–25.05	19938	31	27.45–27.50	12411
10	25.05–25.35	22726	32	27.50–27.55	12537
11	25.35–25.55	20845	33	27.55–27.60	13004
12	25.55–25.75	23048	34	27.60–27.65	12433
13	25.75–25.90	22725	35	27.65–27.70	11686
14	25.90–26.05	24560	36	27.70–27.74	9356
15	26.05–26.20	25724	37	27.74–27.77	6662
16	26.20–26.35	26087	38	27.77–27.80	4163
17	26.35–26.44	21543	39	27.80–27.83	2083
18	26.44–26.53	21591	40	27.83–27.86	1241
19	26.53–26.62	21621	41	27.86–27.89	826
20	26.62–26.71	21230	42	27.89–27.92	651
21	26.71–26.80	19912	43	27.92–27.95	500
22	26.80–26.89	19034	44	27.95–28.00	161

between the observation and the grid point in a particular vertical layer, and  $\delta$  is defined by  $\delta = 0$  if  $|H - H_{obs}| \leq \Delta h$  and  $\delta = 1$  if  $|H - H_{obs}| > \Delta h$  where  $H$  is the ocean depth at the grid point and  $H_{obs}$  is the ocean depth at the data location.

The functional form of  $\Delta h$  has little significance compared to the values imposed by the depth criterion. Therefore, instead of the Gaussian function used by Reynaud et al. (1995), a more tailored polynomial function is used:

$\Delta h = 33x^3 + 90x^2 + 130x + 300$  where  $x$  is defined as  $x = (H - 2000)/1200$ . The actual form was arrived at through many trials, focussing on the representation of the frontal structures along the shelf-break and upper continental slope, where data gradients are much stronger across isobaths than along isobaths.

The third-order polynomial function defined for  $\Delta h$  implies a larger value (approximately 700 m) in the deep ocean and a

smaller value (approximately 190 m) for coastal regions. The advantage of the new depth-dependence function is that a larger range of isobaths is allowed in the calculation of the correction term in deeper waters, where data are scarce, compared to coastal regions where the range of isobaths allowed in the calculation is narrower (Fig. 4).

Smoothing of the final product is carried out in a manner consistent with the modified objective analysis scheme. In other words, using all points within the smallest search radius,  $Q_s = S_{guess_s} - S_{guess_n}$ , and considering the topographic constraints discussed earlier. This was necessary to remove small-scale observational noise which would otherwise disturb the robustness of the climatological property fields.

#### b Diagnostic Calculations

The model used in the diagnostic calculations is a version of the Sub-Polar Ocean Model (SPOM) model developed by Myers (2002), using mean climatological forcing (see Myers (2002) for details). The simplest form of assimilation, direct insertion (e.g., Thompson et al., 2006), is used. This ensures that the model hydrography remains consistent with the climatology at the cost of damping eddies and does not allow the density field to adjust to the circulation. The horizontal resolution of the model is  $1/3^\circ \times 1/3^\circ$ , the same as for the climatology. Therefore, interpolation is not needed in the horizontal but is required in the vertical, where a simple linear interpolation scheme is used to deduce 36 vertical levels of model climatology from the original 44 geopotential layers.

The isopycnal climatology is converted, first, to 44 geopotential layers by using the pressure data, which were objectively mapped onto isopycnal layers as was done with the temperature and salinity data. This first interpolation is necessary in order to compare the two climatologies derived from almost the same data but using different vertical coordinates. Second, the isopycnal climatology (which had been interpolated onto geopotential climate layers) is linearly interpolated onto 36 vertical model levels. As the model domain ( $38^\circ\text{N}$  to  $70^\circ\text{N}$  and  $67^\circ\text{W}$  to  $0^\circ$ ) is larger than that of the climatologies produced here, they are merged with other products covering the rest of the subpolar North Atlantic. For GEO, we use the World Ocean Atlas 1994 (Levitus, 1994), while for ISO we use a modified version of the Lozier et al. (1995) climatology (Grey et al., 1999).

### 4 Climatology

#### a Mean State of the Labrador Sea between 1910 and 2000

The basic elements of the Labrador Sea circulation, such as its fresh and cold boundary currents near the surface, relatively warmer and more saline interior water masses with the DWBC at depth are highlighted in Figs 5a and 5b, which display the climatological  $T$  and  $S$  fields, respectively, along a diagonal cross-section through the Labrador Sea coincident with the frequently occupied World Ocean Circulation Experiment line AR7W. At first glance, one notices the sharp property gradients that separate the WGC on the Greenland

side and the LC on the Labrador side from the less stratified interior. Beneath the surface waters, the interior is filled with waters between the 27.68 and 27.80 isopycnals, part of which is filled with the convectively formed LSW ( $27.74 \leq \sigma_\theta < 27.80$ ). The two density classes, which can be seen below the LSW are the GFZW (associated with the deep salinity maximum) and the DSOW (the deepest waters). The climatological properties of all these water masses are detailed in the following sections.

#### b Surface Fields

The  $T$  (all temperatures reported in this study are potential temperatures referenced to the surface) and  $S$  fields at 30 m (Fig. 6) represent the near-surface water mass distribution. The East Greenland Current (EGC) is only partially resolved in this study, however, its climatological properties near the southern tip of Greenland (approximately  $32.5$  and  $1^\circ\text{C}$ ) create a pronounced gradient with the warm (approximately  $7^\circ\text{C}$ ) and saline (approximately 34.7) IW offshore.

The WGC is described as a mixture of the EGC and IW and hence has slightly higher  $T$  and  $S$  properties than those of the EGC (Clarke, 1984). However, in this analysis the mean annual  $T$  and  $S$  properties of the EGC and the WGC are found to be almost the same (approximately  $32.5$  and  $1^\circ\text{C}$  for both water masses). These  $T$  and  $S$  values are less than the ones reported in the Reynaud climatology and closer to the observed values (Clarke, 1984). The northern WGC, entering Davis Strait and Baffin Bay, however, seems to be more saline and warmer than farther south, with a temperature of approximately  $2.5^\circ\text{C}$  and a salinity of 33 at approximately  $65^\circ\text{N}$ . However, this increase is more likely to be caused by the summer bias in the data than mixing with other water masses.

The density gradient between the fresh water near the coast and the IW is maintained during the objective mapping due to two factors, each of which avoids excessive smoothing. One factor is the smaller range of depths over which the correction term is calculated, and this separates the relatively warmer and more saline waters offshore from the cold and fresh WGC. The second factor is the use of isopycnal coordinates in the vertical, which will be discussed further. Subsurface temperature maxima associated with the IW at approximately 150 m on the Greenland side is noticeable in Fig. 5a. It is well documented in the literature (e.g., Clarke, 1984; Cuny et al., 2002) that IW enters the Labrador Sea from the east and exits to the south after circulating cyclonically around the basin.

Two distinct current branches carry water northward across  $60^\circ\text{N}$  along the west Greenland shelf and slope (Fig. 7b). The offshore branch seems to be carrying the warm and saline IW while the inshore branch contains fresh and cold water from the WGC. Furthermore, while the WGC continues to flow northward, a considerable amount of warm and saline IW mixes into the interior Labrador Sea.

The southern cross-sectional property map (Fig. 8b) shows a subsurface temperature minimum at approximately 80 m between  $54^\circ$  and  $51.5^\circ\text{W}$ , with a temperature of  $-1^\circ\text{C}$ , which

## Comparing Two Climatologies of the Labrador Sea: Geopotential and Isopycnal / 27

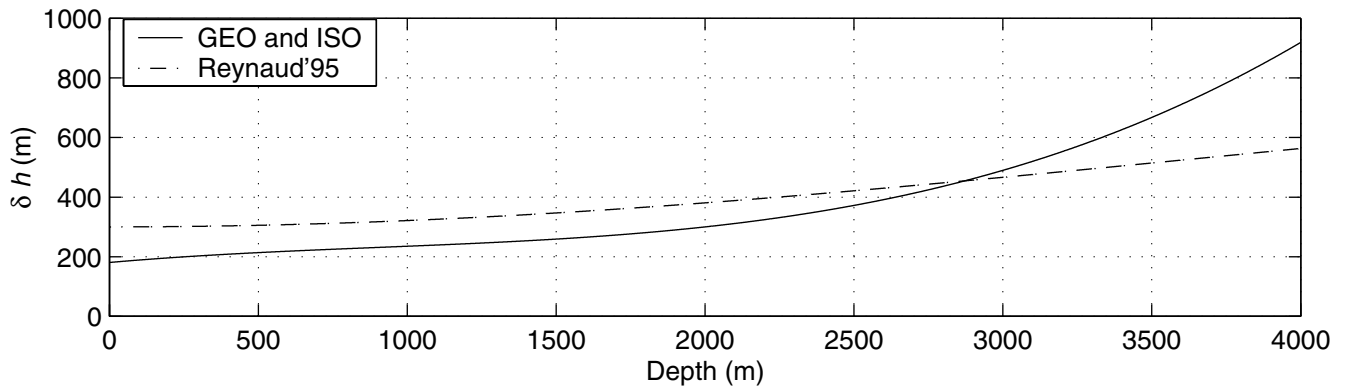


Fig. 4 Plot showing the different  $\delta h$  values used in the objective analysis for the polynomial approach used in this work compared to the Gaussian function used in Reynaud et al. (1995).

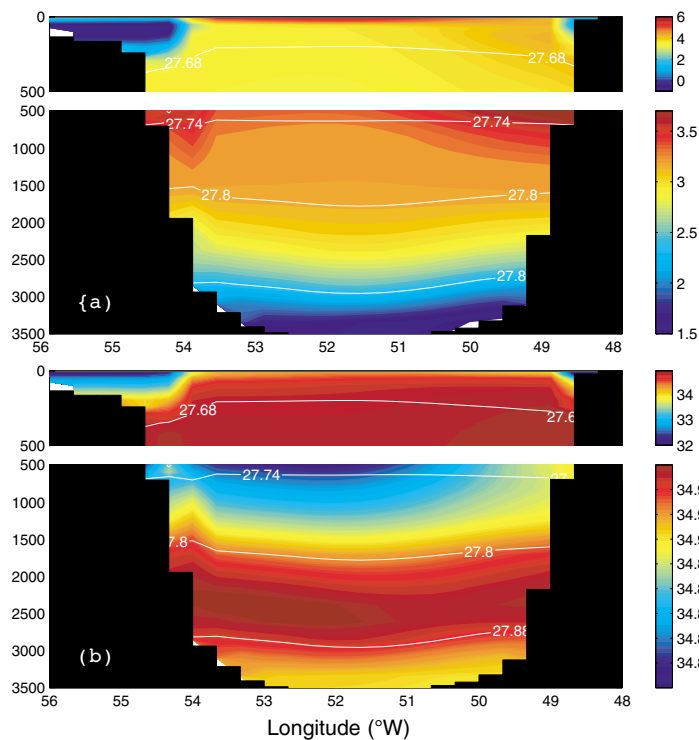


Fig. 5 Cross-section of a) potential temperature and b) salinity from ISO for a diagonal cross-section across the Labrador Sea (shown on Fig. 1). The 27.68, 27.74, 27.80 and 27.88 isopycnals are shown in white.

is cooler than the minimum temperature for the LC farther north and is consistent with the premise that the cold intermediate layer is most prominent along the southern part of the Labrador shelf (Myers et al., 1990). The two branches of the LC to the south of Hamilton Bank are described by Lazier and Wright (1993) and can be identified in Fig. 8b. The offshore branch is mainly barotropic with an average southward velocity of  $10 \text{ cm s}^{-1}$  throughout the water column and centred over the 2500 m isobath as described by Lazier and Wright (1993). The baroclinic component of the LC is concentrated in the top 200 m or so and located inshore of the barotropic component.

The mean salinity of the LC (approximately 33.7 for the top 300 m) is slightly less than that of the WGC. Below this

fresh and cold boundary current, a salinity maximum is observed centred around 450 m (not shown). This maximum is caused by the IW that enters the Labrador basin from the east on the Greenland side at approximately 150 m, crosses  $60^\circ\text{N}$  latitude southward at approximately 200 m, and is found at approximately 450 m at  $53^\circ\text{N}$ , which gives a rate of descent of  $3.5 \times 10^{-4}$  for the IW core depth as it flows cyclonically around the basin.

### c Intermediate to Deep Water Masses

Mean temperature and salinity values for the LSW are found to be approximately  $3.2^\circ\text{C}$  and approximately 34.89, respectively from ISO between the potential density layers of 27.74

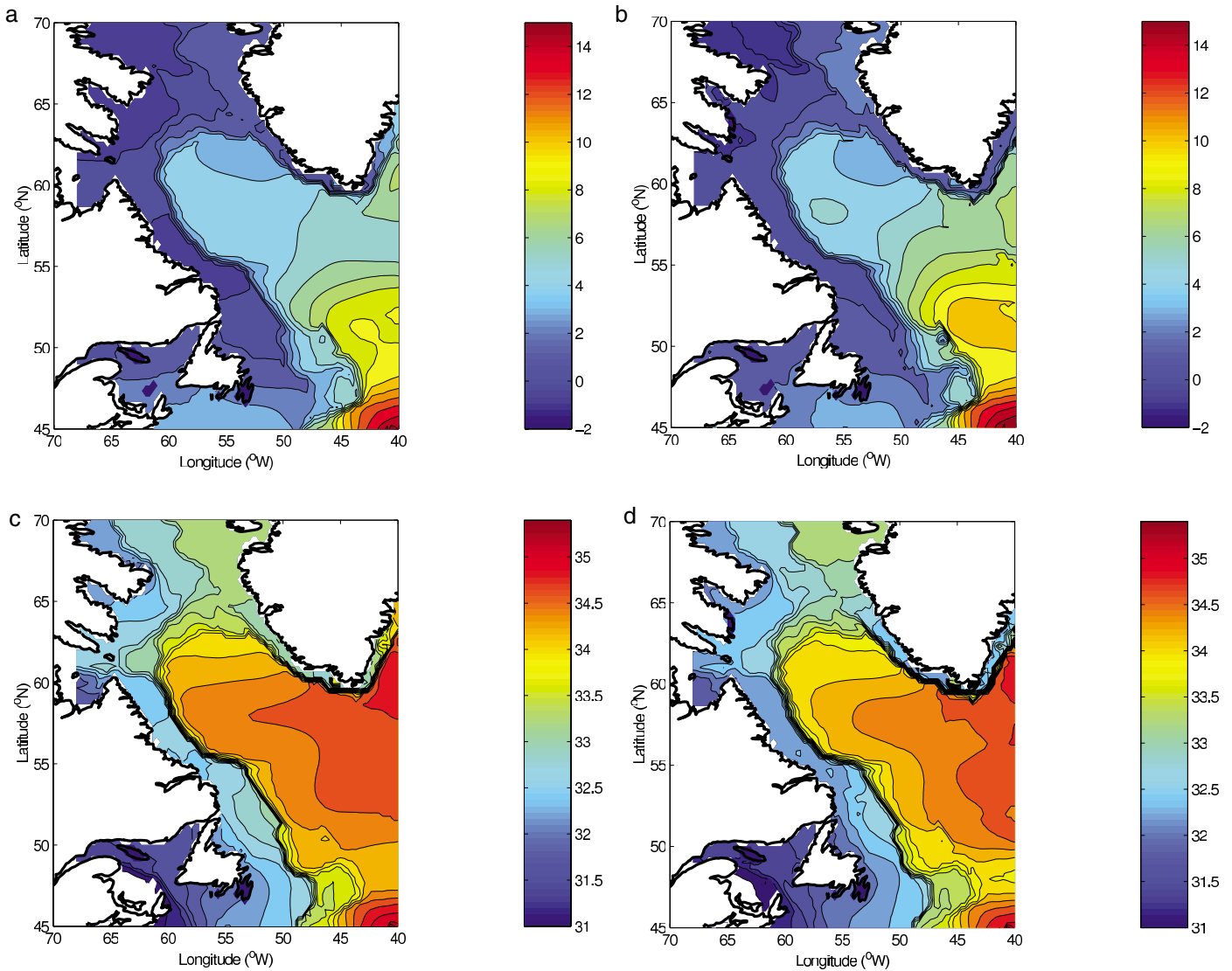


Fig. 6 30 m plots for each of our two climatologies showing temperature for a) GEO and b) ISO; and salinity for c) GEO and d) ISO.

and 27.80 (Fig. 5). These values compare well to the  $T$  and  $S$  properties attributed to the LSW over the years (e.g., 3.4°C and 34.89 by Lazier (1973) and 2.8°C and 34.89 by Clarke and Gascard (1983). Considering waters with potential densities less than 27.80, the climatological maximum depth for LSW appears to be approximately 1700 m, consistent with the estimates of Lilly et al. (1999). During periods of restratification, the gradient region between LSW and the GFZW becomes thicker and more diffuse. Data smoothing from the climatological analysis has the same effect. Therefore the climatological realization here presents more of an average description of the properties than that which may exist at any one time.

The DWBC enters the Labrador Sea from the east, circulates cyclonically around the Labrador Sea and exits at the south. The depth at which the lighter component of the DWBC, the GFZW, enters the Labrador Sea is slightly shallower (2300 m) than the depth at which it exits (2400 m). The

salinity maximum of the GFZW of approximately 34.93 can be seen hugging the Labrador rise at 2400 m. Below this density layer, the DSOW is fresher (34.91) but colder (1.7°C). Dickson et al. (2002) suggested that the salinity of the deep water masses in the Labrador Sea fluctuates between 34.95 and 34.90 for the GFZW, and between 34.91 and 34.88 for the DSOW, considering measurements between the early 1960s and the late 1990s. The new climatologies put the long-term (1910-2000) mean annual salinity of these water masses closer to the upper bound of the range mentioned by Dickson et al. (2002).

#### **d** Justification of the Choice of Isopycnal Climatology

In this section the results from ISO and GEO are compared to each other, and their relative strengths and weaknesses are discussed. We start by examining the large-scale, long-term average water properties for three regions: the interior of the Labrador Sea, the WGC and the LC (Fig. 1). Heat and

freshwater content is calculated according to the following formulae:  $H = c_p \rho_o \int_V (T - T_r) dV$  where  $c_p = 4000 \text{ J kg}^{-1} \text{ } ^\circ\text{C}^{-1}$  is the specific heat of water;  $\rho = 1000 \text{ kg m}^{-3}$  is the reference density;  $V$  is the volume;  $T$  is the climatological temperature; and  $T_r = 0^\circ\text{C}$  is the reference temperature.

$$FW = \int_V \frac{S_r - S}{S_r} dV$$

where  $S$  is the climatological salinity, and  $S_r = 35$  is the reference salinity. Tables 4 and 5 summarize some of the important parameters.

In ISO, although the mean temperatures are higher than for GEO, the gradients in temperature between the boundary currents and the interior are larger. The boundary current salinities are also fresher in ISO, being on average approximately 0.1 fresher through the top 300 m than in GEO. One possible explanation for these differences is that ISO uses isopycnal averaging over steep isopycnal slopes, as in the case of boundary currents in the Labrador Sea, both on the Labrador and Greenland side. By doing so, the ISO climatology avoids the smearing of the shelf-break fronts. Hence, the characteristics of the different water masses are better preserved. It must also be noted that isopycnal averaging has problems near the surface associated with the appearance and disappearance of layers throughout the seasonal cycle.

The boundary currents concentrated over the continental slope can be identified from the high current velocities near the surface (Fig. 8). The surface velocities calculated from ISO are as large as  $20 \text{ cm s}^{-1}$  in the inshore (baroclinic) branch of the LC. Even though the GEO velocities are comparable to the ISO velocities near the surface, they are much less barotropic, decaying rapidly with depth. Deep velocities are nearly twice as fast in ISO than GEO. In order to show the jet structures more closely, ‘pointwise’ transports as well as the net transports are plotted in Figs 9a and 9b. Total annual mean transport is  $46.6 \text{ Sv}$  in ISO compared to  $26.1 \text{ Sv}$  in GEO. The ISO value is consistent with previous diagnostic estimates for the subpolar gyre, such as those of Reynaud, (1994), Reynaud et al. (1995) and Myers et al. (1996). Consistent with the barotropic nature of the velocities in ISO, the total transport is reasonably evenly divided between the layers. The broadening of the jet and associated weakening of the transport can also be clearly seen in a plot of sea surface height from the diagnostic model (Fig. 9c). The GEO simulations show only a weak and broad northward flow offshore of the Labrador Current, while in ISO this feature is stronger and more defined, around  $44^\circ\text{W}$ .

Perhaps the most striking difference between the ISO and GEO property fields is, however, the location of the DWBC. The maximum in salinity associated with the DWBC is located at approximately 2000–2500 m in both climatologies, but the salinity signature is more defined and centred over the continental slope off Labrador in ISO (Fig. 8). Additionally, the deep salinity maximum markedly decreases as it approaches the intersection with the bottom. Since both climatologies use the same depth-dependence criterion, this dif-

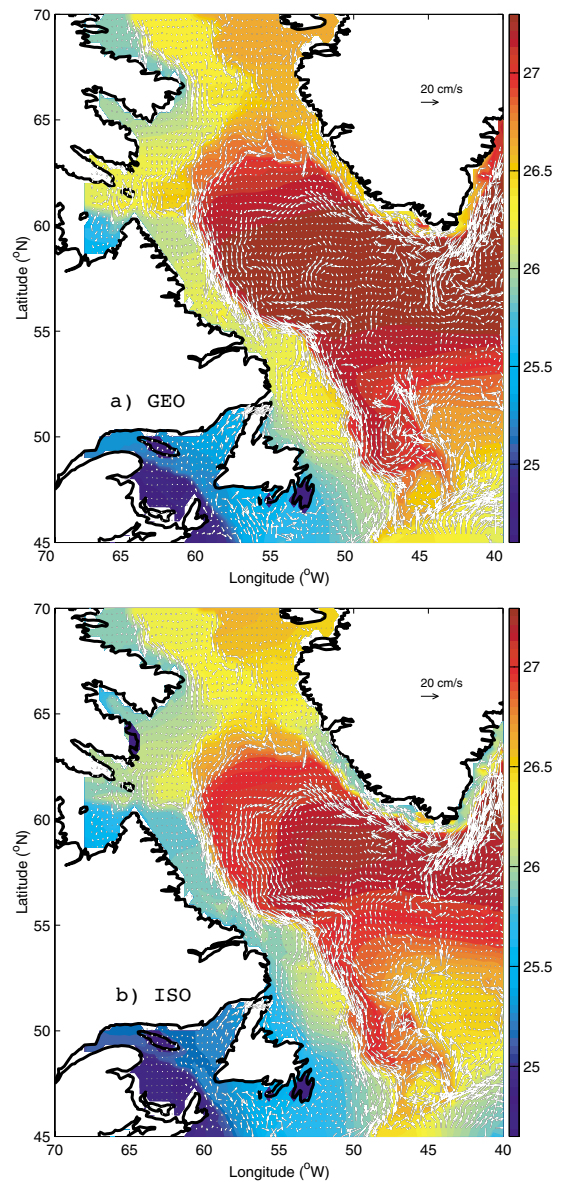


Fig. 7 Plots of density at 30 m depth with currents from the diagnostic model superimposed for a) GEO and b) ISO.

ference must be a consequence of the vertical averaging method, i.e., the use of geopotential versus isopycnal coordinates in the vertical. Since the baroclinic nature of the DWBC is not well preserved in GEO, the current velocities and volume fluxes calculated from this climatology are underestimated (Fig. 8).

A comparison of ISO- and GEO-based volume fluxes and with flux estimates from the Lowered Acoustic Doppler Current Profiler (LADCP) used by Fischer et al. (2004) and Dengler et al. (1002) is given in Table 6. The agreement between the ISO volume fluxes and the LADCP measurements is remarkable considering the differences in transect alignment, in approaches, in the periods covered by this study (1910–2000) and the studies by Fischer et al. (2004) (1996–2001) and Dengler et al. (2006) (1996–2003). On the other

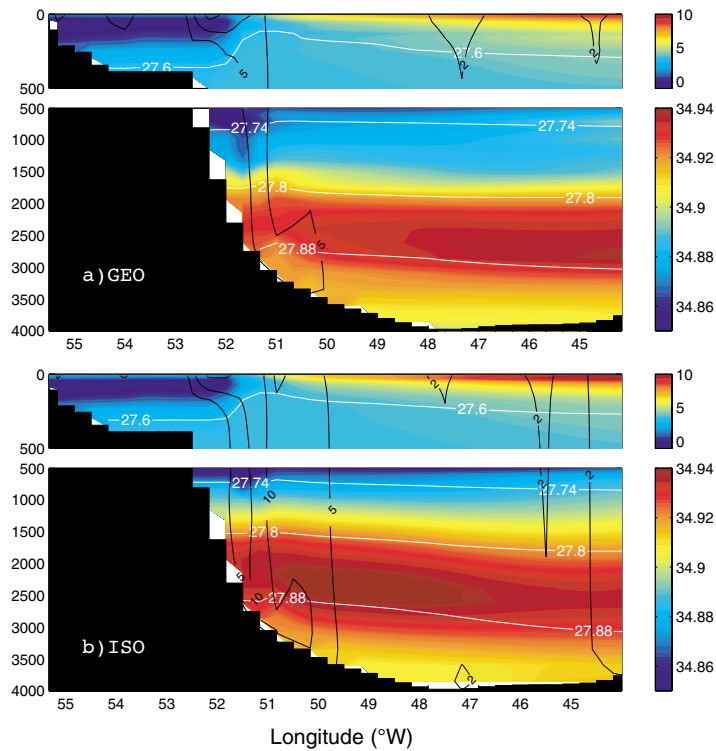


Fig. 8 Section at 53°N for a) GEO and b) ISO, with the upper panel in each pair showing potential temperature and the lower panel showing salinity. Velocities from the diagnostic model are superimposed with contour intervals of  $-15 \text{ cm s}^{-1}$ ,  $-10 \text{ cm s}^{-1}$ ,  $-5 \text{ cm s}^{-1}$  and  $2 \text{ cm s}^{-1}$  plotted.

TABLE 4. A list of mean water properties and total freshwater and heat content for the Labrador Current, West Greenland Current and interior regions, for a series of depth ranges, for the mean annual GEO climatology.

Depth range (m)	Region	$S_{mean}$	$\theta_{mean}$ (°C)	$\sigma_{\theta}$	$\Sigma FW$ ( $\text{m}^3$ )	$\Sigma H$ ( $GJ$ )
0–300	LC	33.90	2.21	27.07	$1.9 \times 10^{12}$	$5.4 \times 10^{11}$
	WGC	34.57	3.04	27.53	$2.9 \times 10^{11}$	$2.8 \times 10^{11}$
	Interior	34.56	3.09	27.52	$1.4 \times 10^{12}$	$1.3 \times 10^{12}$
0–1500	LC	34.55	3.01	27.52	$2.4 \times 10^{12}$	$2.2 \times 10^{12}$
	WGC	34.80	3.48	27.68	$4.2 \times 10^{11}$	$1.0 \times 10^{12}$
	Interior	34.82	3.38	27.71	$2.7 \times 10^{12}$	$7.3 \times 10^{12}$
0–3000	LC	34.64	2.96	27.60	$2.5 \times 10^{12}$	$2.9 \times 10^{12}$
	WGC	34.82	3.41	27.70	$4.4 \times 10^{11}$	$1.1 \times 10^{12}$
	Interior	34.88	2.95	27.79	$3.8 \times 10^{12}$	$1.3 \times 10^{13}$
0–>3000	Interior	34.88	2.85	27.80	$4.1 \times 10^{12}$	$1.3 \times 10^{13}$

hand, GEO consistently underestimates the volume fluxes by about a factor of two except perhaps for the deepest layer.

#### e Comparison of the New Climatology with Existing Climatologies

One of the aims of this study was to build an improved climatology for the Labrador Sea. Several large-scale ocean climatologies based on geopotential (Levitus, 1994) and isopycnal (Lozier et al., 1995) coordinates are compared with the GEO and ISO climatologies produced here. We also consider the higher resolution 1/4 degree version of the World Ocean Atlas 2001 (Boyer et al., 2005). We also examined the

newer World Ocean Atlas 2005 but found few differences between it and the Levitus (1994) fields we used here for our comparisons.

Increased horizontal and vertical resolution, smaller search radii of iterations, and the application of a depth-dependant OA scheme successfully preserved the shelf-break fronts (Figs 7a and 7b). The differences between the larger scale climatologies (e.g., Fig. 10) and the current ones (e.g., Fig. 6) are remarkable, especially near the fronts and boundary currents.

Examining the sea surface height (SSH) fields calculated from the diagnostic model at the 53°N section (Fig. 9c),

TABLE 5. As in Table 4, but for the mean annual ISO climatology.

Depth range (m)	Region	$S_{mean}$	$\theta_{mean}$ (°C)	$\sigma_{\theta}$	$\Sigma FW$ (m <sup>3</sup> )	$\Sigma H$ (GJ)
0–300	LC	34.07	2.21	27.20	$1.9 \times 10^{12}$	$6.2 \times 10^{11}$
	WGC	34.51	3.70	27.42	$4.8 \times 10^{11}$	$5.1 \times 10^{11}$
	Interior	34.73	3.93	27.58	$8.3 \times 10^{11}$	$1.7 \times 10^{12}$
0–1500	LC	34.64	3.10	27.58	$2.5 \times 10^{12}$	$3.0 \times 10^{12}$
	WGC	34.82	3.74	27.67	$7.4 \times 10^{11}$	$2.1 \times 10^{12}$
	Interior	34.86	3.52	27.72	$2.2 \times 10^{12}$	$7.6 \times 10^{12}$
0–3000	LC	34.70	3.05	27.64	$2.7 \times 10^{12}$	$3.8 \times 10^{12}$
	WGC	34.84	3.58	27.70	$8.1 \times 10^{11}$	$2.5 \times 10^{12}$
	Interior	34.89	3.11	27.79	$3.3 \times 10^{12}$	$1.3 \times 10^{13}$
0–>3000	Interior	34.89	3.00	27.80	$3.6 \times 10^{12}$	$1.4 \times 10^{13}$

reveals, once more, how these larger scale climatologies broaden the front and the associated LC. Examining these fields spatially (not shown) shows a broad and deep subpolar gyre depression for the Levitus (1994) and Lozier et al., (1995) estimates (with somewhat tighter features in Lozier). Besides the tighter gradients at the shelf-break, both GEO and ISO have a shallower large-scale depression of the sea surface in the interior. Instead the maximum depression is associated with smaller recirculation cells offshore of the LC (better represented in ISO). Where these recirculation cells are present, the sea surface depression/transport in ISO exceeds that in GEO, and approaches that found in Levitus/Lozier, such as shown at 53°N.

Looking along a section south from Cape Farewell at 44°W (Fig. 11a), all four climatologies represent the inflowing EGC, albeit with different strengths and structures, but only the two climatologies developed in this study include outflow centred at 56°N. Looking at this last feature in more detail in ISO (Fig. 11b) shows that it is mainly associated with a flux of waters with densities between 27.68 and 27.80 out of the Labrador Sea (i.e., the export of LSW). The difference may be related to the larger smoothing scales in Lozier's analysis, or the lack of data in the analysis from the mid- to late 1990s when there was an anomalously large volume of LSW and consequently a larger than average outflow. The ISO estimate of -41.2 Sv transported into the Labrador Sea north of 57°N is comparable to the estimate of Clarke (1984) of -33.5 Sv on the Greenland Slope.

**f Freshwater Transport**

Total southward freshwater transport in the LC (Fig. 12a) is 239 mSv (with respect to a reference salinity of 35.0), with almost 60% of this carried in the upper layer. The upper layer component is reasonably equally divided between the shelf, shelf-break and slope branches of the current. This is somewhat larger than the Loder et al. (1998) estimate of 189 mSv for the Seal Island Transect, albeit that section does not reach as far offshore as the maximum determined here. Import to the Labrador Sea from the east in the EGC (Fig. 12b) is 129 mSv, which is divided reasonably equally among all lay-

ers. This is much larger than the 29 mSv estimated passing Cape Farewell by Loder et al. (1998) but potentially consistent with the recent estimate of  $60.2 \pm 20.5$  mSv in the WGC crossing a line at Cape Desolation (Myers et al., unpublished manuscript).

**5 Seasonal Analysis**

Seasonal variability is the fundamental mode of variability in the ocean-atmosphere system. The Labrador Sea undergoes remarkable changes in its freshwater and heat content, which regulate winter convection and restratification. This section is therefore dedicated to the intra-annual variability of the freshwater and heat budgets of the Labrador Sea interior, WGC and LC system. The seasons are defined here as winter (January–March), spring (April–June), summer (July–September) and fall (October–December).

The amount of fresh water and heat stored in the central Labrador Sea undergoes substantial changes throughout the year. Tables 7–10 list the total freshwater and heat content, and the mean temperature, salinity and density of the top 300, 1000 and 2000 m. The total freshwater content in all four depth classes of the water column reaches its maximum in fall, except in the WGC, where the freshwater content peaks earlier, in summer. Another exception is the freshwater content of the top 1500 m of the LC, which does not show a significant change between fall and winter. The heat content of the top 3000 m in all three regions peaks in the fall.

Near-surface water properties are the least affected by the temporal bias as there is usually an adequate number of observations from every decade. Therefore an average ocean-to-atmosphere heat flux over the cooling season can be calculated from the seasonal heat content of the top 1000 m by assuming that the heat content change is derived from a heat flux to the atmosphere. Steffen and D'Asaro (2002) used this method to calculate the atmospheric heat flux based on data collected using profiling floats. For 1998, they estimated that the heat lost to the atmosphere was approximately  $140 \pm 50$  W m<sup>-2</sup>. Lavender et al. (2002) used float-based measurements to estimate winter heat losses over the top 400 m of the convection region of 188 W m<sup>-2</sup> for 1997 and 148 W m<sup>-2</sup>

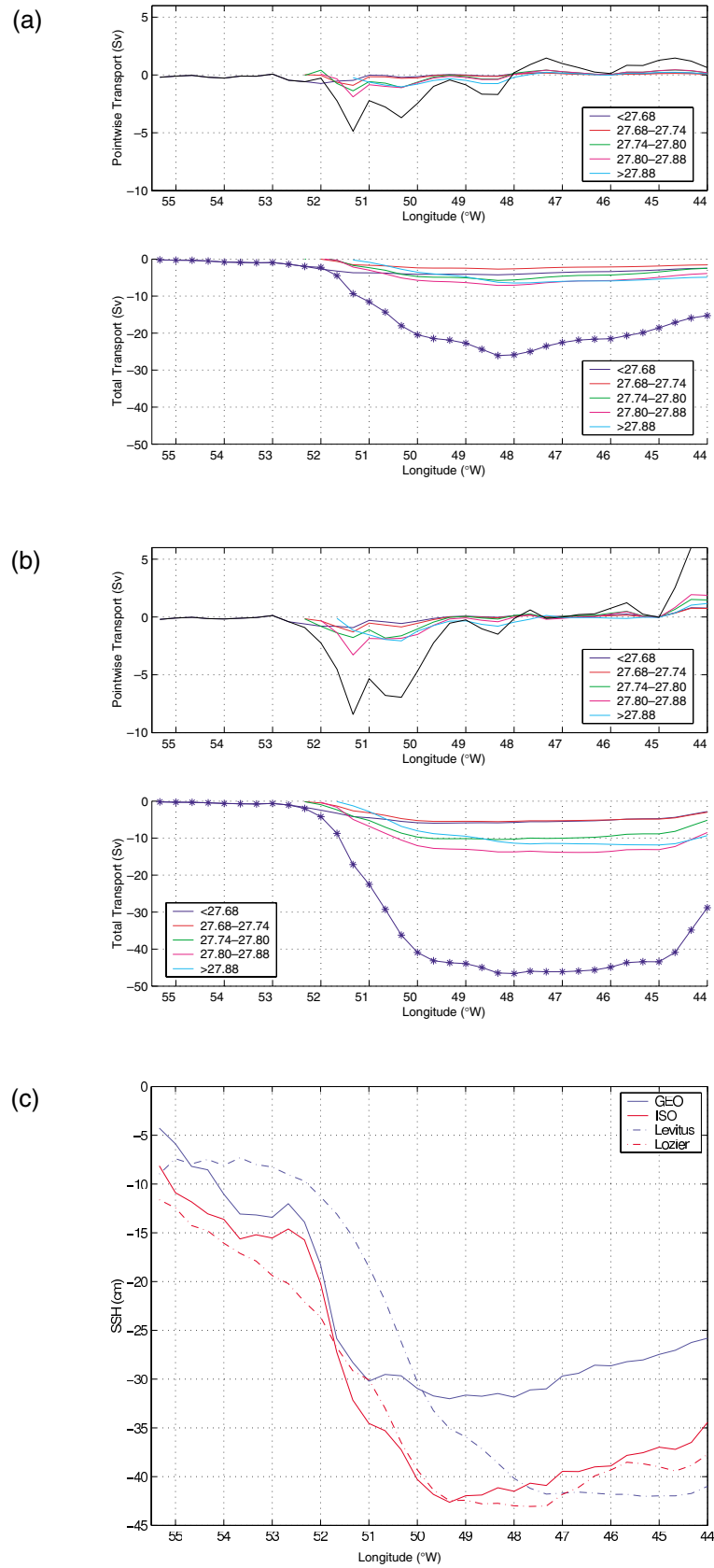


Fig. 9 a) Volume transport across 53°N (total and for 5 density layers) from GEO, with the top panel showing ‘pointwise’ transport for a column at the given longitude (black curve is the total over the water column) and the lower panel showing the accumulated total transport from the coast (the line with blue stars is the total transport over the water column.). b) As in Fig. 9a but for ISO. c) Sea surface heights from the diagnostic model at 53°N.

TABLE 6. Volume fluxes calculated from the GEO and ISO climatologies along a section at 53°N are compared to the LADCP-based fluxes reported by Fischer et al. (2004). The potential density ranges in the first column correspond to LSW, GFZW, and DSO. Volume transports are in Sverdrups.

Density Range	GEO	ISO	LADCP <sup>1</sup>	LADCP <sup>2</sup>
$\sigma_\theta < 27.74$	-6.1	-13.5	-12.3	-13.3
$27.74 \leq \sigma_\theta < 27.80$	-3.8	-15.3	-10.7	-18.3
$27.80 \leq \sigma_\theta < 27.88$	-5.2	-7.2	-9.4	-8.9
$\sigma_\theta < 27.88$	-3.7	-7.4	-5.3	-3.8

<sup>1</sup>taken from Fischer et al. (2004) Fig. 5a.

<sup>2</sup>taken from Dengler et al. (2006) Fig. 3d.

for 1998. Here climatological heat content values for fall (representing prior to convection) and winter (representing just after convection) are used. We arrive at a net heat flux of approximately  $-120 \text{ W m}^{-2}$ . Since we effectively considered only a cooling season of mid-November to mid-February (rather than the full winter of October to March defined by Smith and Dobson (1984), it is not surprising that our estimate is lower. Additionally, this can be compared to an estimated heat loss of  $-207 \text{ W m}^{-2}$  from the interior of the Labrador Sea computed from the National Centers for Environmental Prediction/National Center for Atmospheric Research (NCEP/NCAR) reanalysis data, based on the years 1948–97, although Renfrew et al. (2002) show that the NCEP/NCAR reanalysis data significantly overestimate the latent and sensible heat loss in the Labrador Sea.

Since we find that the upper limit of the LSW density layer is located at almost the same depth in winter and fall, the volume of newly produced LSW between these two seasons can be estimated by the deepening of the lower limit of the LSW density layer between these two seasons, which is approximately 70 m. Taking into account the area that we define as the interior of the Labrador Sea ( $4 \times 10^5 \text{ km}^2$ , Fig. 1), the additional LSW produced during convection is estimated to be  $28,000 \text{ km}^3$ , which corresponds to a volume flux of approximately 3.6 Sv. Taking into account only the difference in volume between the upper and lower limits of LSW density between the fall and spring climatologies for the Labrador Sea where the water depth is at least 3000 m gives a formation rate of 3.8 Sv. This is comparable to a rate of 4.4–5.6 Sv for the period 1970–97 estimated by Rhein et al. (2002) based upon the CFC-11 inventory. Additionally, Boning et al. (2003) estimated LSW formation rates using an eddy-permitting ocean general circulation model with respect to the period 1959–97 and calculated, using the same CFC inventory method of Rhein et al. (2002), a formation rate of 3.4–4.4 Sv.

## 6 Summary

Two climatologies, one using isopycnic layers and the other employing a more classical geopotential approach, are produced for the Labrador Sea region. Compared to existing climatologies, smaller search radii, more data and a depth-dependent correction scheme are used. The result is the

preservation of the strong fronts that exist between cold and fresh boundary currents and warmer and more saline interior waters and, in general, less smoothing of features (Fig. 6). The waters of the WGC, LC and the interior are well represented, especially the LSW and the DWBC.

We estimate the total transport of the Labrador Current/subpolar gyre at 53°N as 46.6 Sv southward, with 9.7 Sv of that being LSW, 12.1 Sv being GFZW and 8.0 Sv being DSO. Transport into the Labrador Sea by the EGC is 41.2 Sv with 6.6 Sv of LSW exported back to the Irminger Sea south of 57°N. Total southward freshwater transport by the Labrador Current (including slope and 'gyre' branches) is 239 mSv at 53°N, with almost 60% of this carried in the upper layer. Import of fresh water to the Labrador Sea from the east in the EGC is 129 mSv, which is divided relatively equally among all layers. Our estimate of the long-term mean formation rate of LSW is between 3.6 and 3.8 Sv based on simple volume and isopycnal depth change ideas.

One can ask why another climatology of the Labrador Sea is needed, as a number already exist. However, when this study was started, no fully usable and up-to-date high resolution climatology of the Labrador Sea was available and described in the literature. The most recent was that of Reynaud et al. (1995) which used geopotential averaging in the vertical. This last is also a key point, for although Lozier et al. (1995) showed the advantages of an isopycnal approach for the global ocean, this idea needed to be expanded upon for localized regions using higher resolution. Thus, we compare and contrast the resulting Labrador Sea climatologies using the geopotential and isopycnal approaches in this work.

We find that the isopycnal climatology produces the best results. Isopycnal averaging gives more realistic results by avoiding artificial mixing of water properties and preserving the baroclinicity of the flow. As well, when the climatological data are used in a diagnostic model to calculate velocities (and thus transports), the estimates from the isopycnal analysis are much closer to other observational and modelling studies. It could be argued that the extreme interannual to interdecadal variability in the Labrador Sea, whereby isopycnal layers significantly change in depth with time, makes such an approach unfeasible for long-term analysis in this region. Although we would agree that this is a potential issue, we think this variability will affect any climatology, even one using geopotential coordinates. Other issues with our isopycnal analysis include our choice of density ranges for isopycnal layers which might be too thick around the convection site and patchiness near the surface caused by the interpolation of isopycnal coordinates back to geopotential coordinates for presentation (and use in the diagnostic model).

Finally, if one wants to use such a product to analyze variability in the Labrador Sea and to initialize (or assimilate into) models, one first needs to show that the climatology does a good job of representing the major water masses of the region, including the boundary currents, the tight fronts on the shelf-break and the interior. And, at least in our opinion, it is important to present this baseline as a separate study, with the

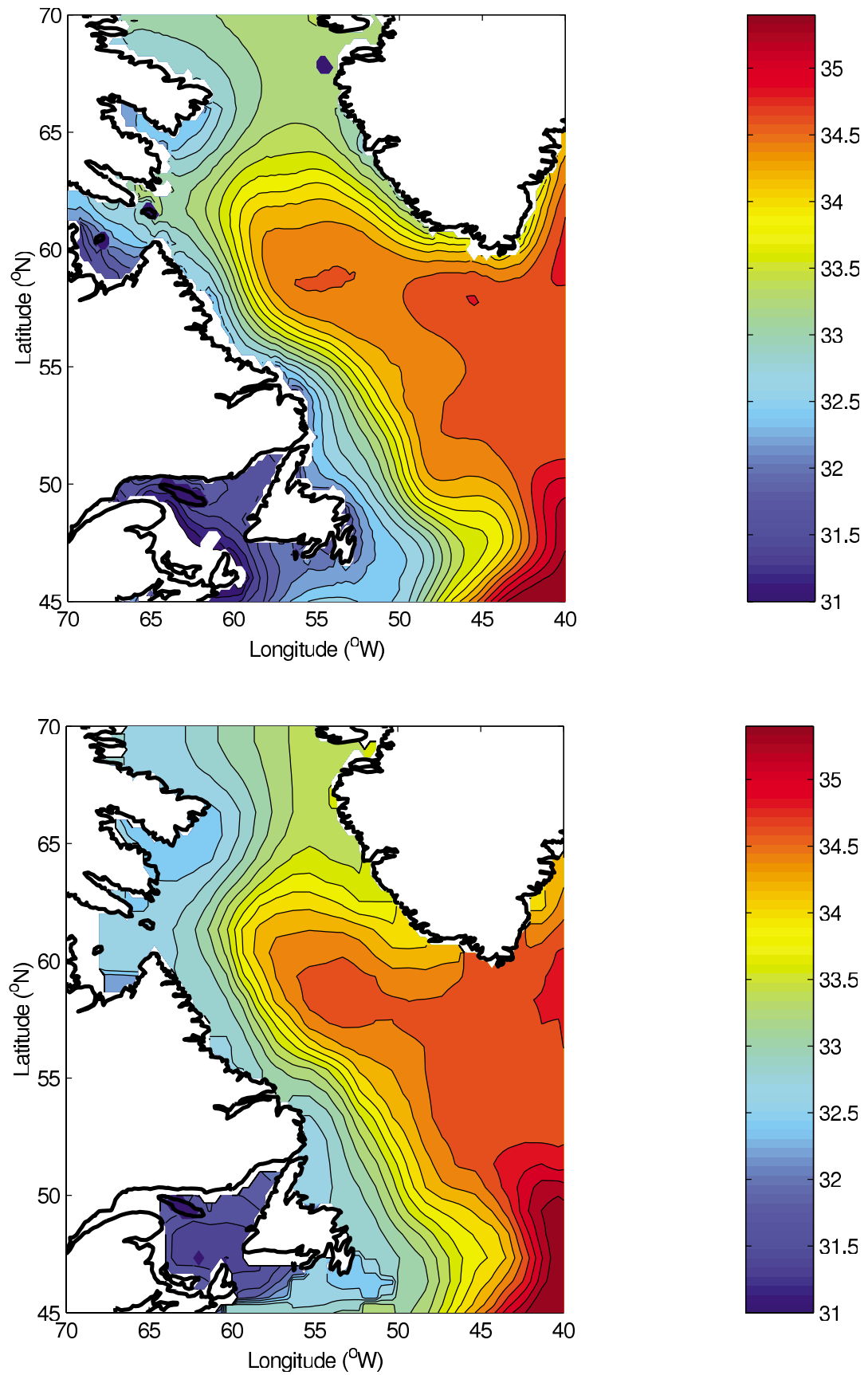


Fig. 10 Salinity at 30 m plotted from a) the 1/4 degree WOA01 and b) the Lozier et al. (1995) climatology.

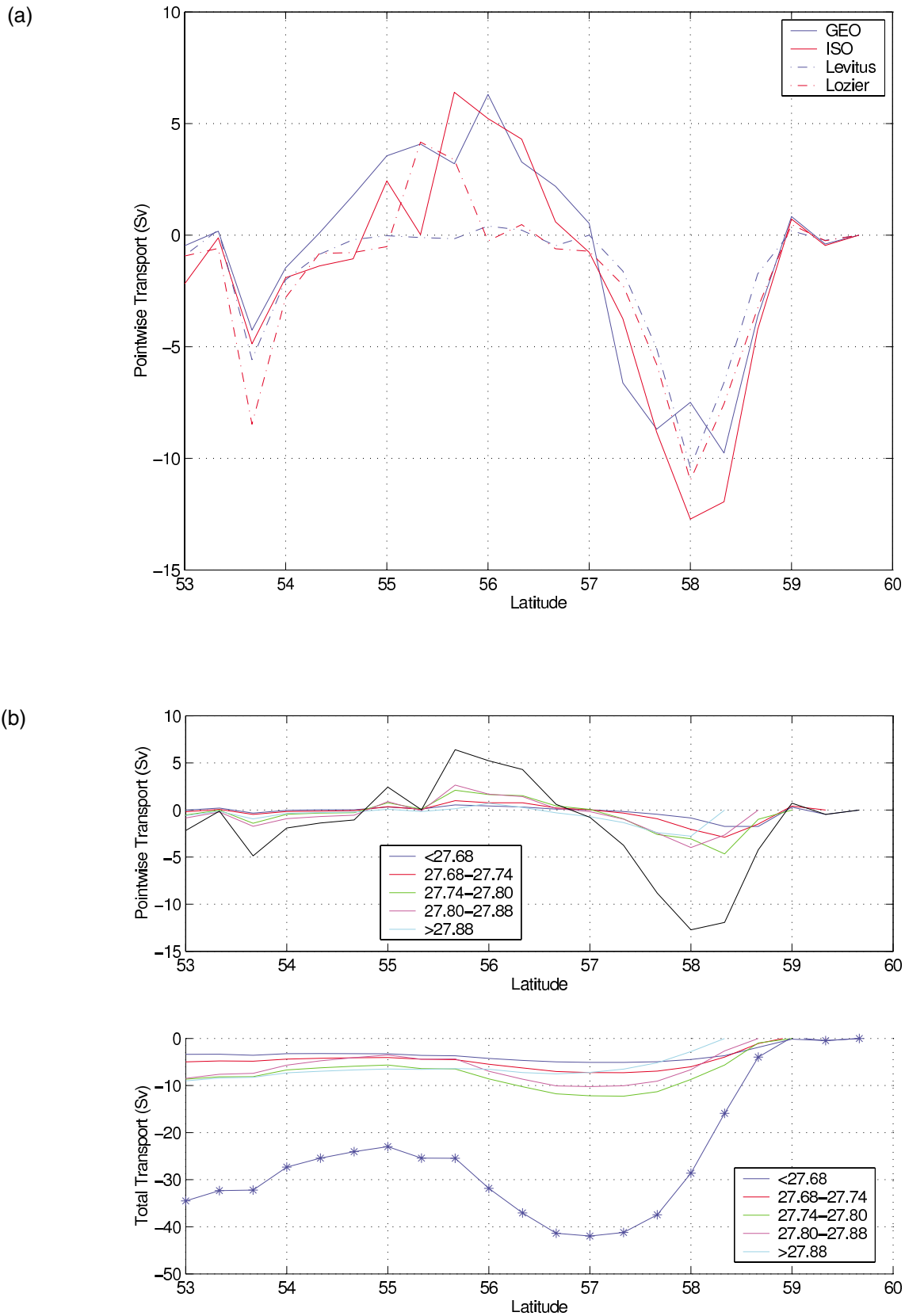


Fig. 11 a) 'Pointwise' volume transport for a column at the given latitude along 44°W and b) volume transport across 44°W (total and for five density layers) from ISO, with the top panel showing 'pointwise' transport for a column at the given longitude and the lower panel showing the accumulated total transport from the coast.

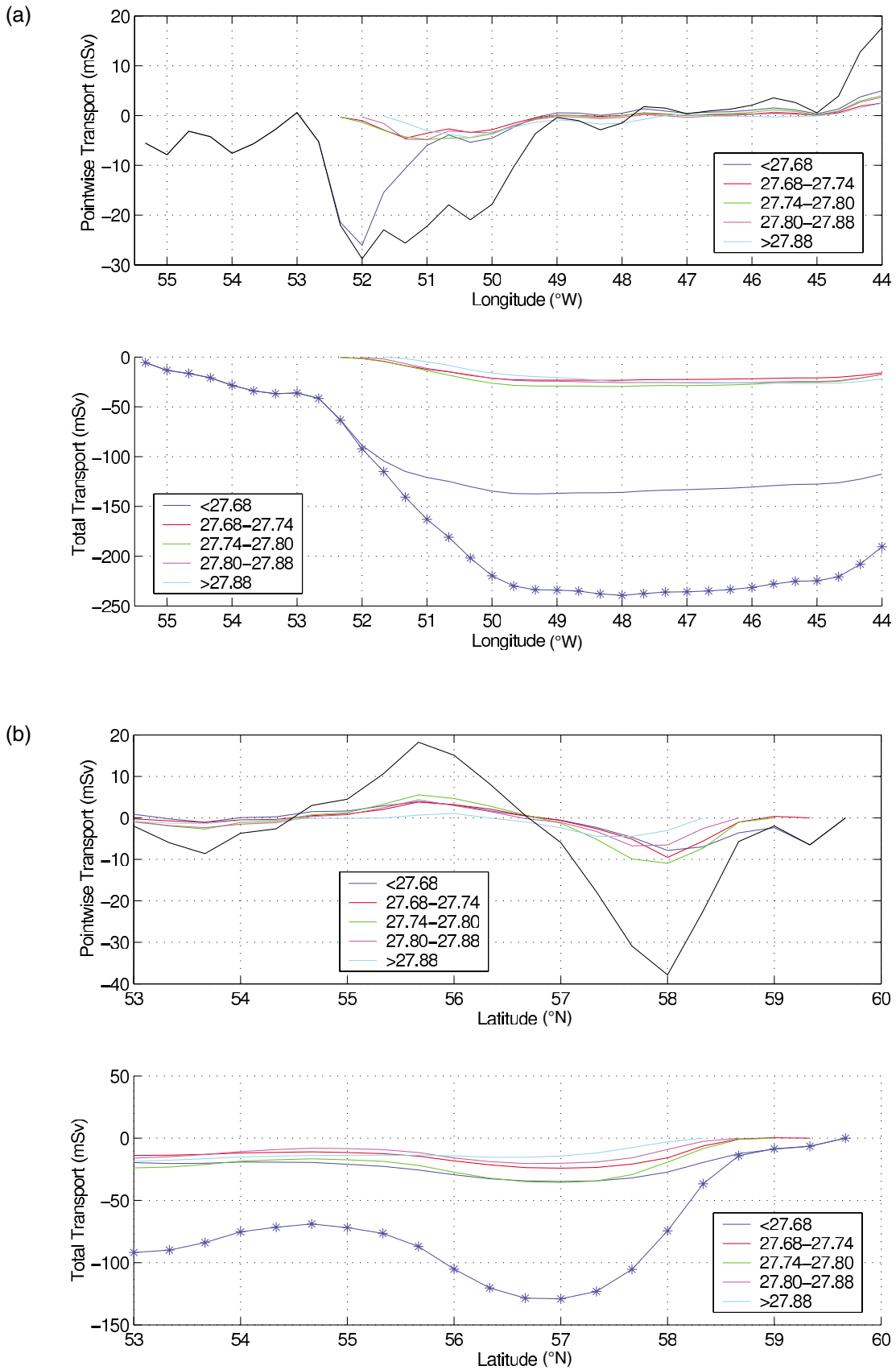


Fig. 12 Freshwater transport across a) 53°N and b) 44°W, from ISO, with the top panel in each case showing the pointwise transport (for the entire water column and each of five density layers) and the lower panel showing the accumulated total freshwater transport from the coast for those same layers.

## Comparing Two Climatologies of the Labrador Sea: Geopotential and Isopycnal / 37

TABLE 7. As in Table 4, but for the spring ISO climatology.

Depth range (m)	Region	$S_{mean}$	$\theta_{mean}$ (°C)	$\sigma_{\theta}$	$\Sigma FW$ (m <sup>3</sup> )	$\Sigma H$ (GJ)
0–300	LC	33.96	1.56	27.16	$1.88 \times 10^{12}$	$3.96 \times 10^{11}$
	WGC	34.30	2.72	27.35	$6.39 \times 10^{11}$	$3.49 \times 10^{11}$
	Interior	34.67	3.53	27.57	$1.10 \times 10^{12}$	$1.64 \times 10^{12}$
0–1500	LC	34.49	2.60	27.50	$2.12 \times 10^{12}$	$1.51 \times 10^{12}$
	WGC	34.71	3.43	27.61	$7.83 \times 10^{11}$	$1.28 \times 10^{12}$
	Interior	34.84	3.39	27.72	$2.39 \times 10^{12}$	$7.00 \times 10^{12}$
0–3000	LC	34.67	2.66	27.56	$2.19 \times 10^{12}$	$1.89 \times 10^{12}$
	WGC	34.75	3.34	27.65	$8.18 \times 10^{11}$	$1.51 \times 10^{12}$
	Interior	34.88	3.08	27.78	$3.52 \times 10^{12}$	$12.71 \times 10^{12}$
0–>3000	Interior	34.88	2.96	27.79	$3.80 \times 10^{12}$	$13.47 \times 10^{12}$

TABLE 8. As in Table 4, but for the summer ISO climatology.

Depth range (m)	Region	$S_{mean}$	$\theta_{mean}$ (°C)	$\sigma_{\theta}$	$\Sigma FW$ (m <sup>3</sup> )	$\Sigma H$ (GJ)
0–300	LC	33.75	1.86	26.97	$2.29 \times 10^{12}$	$4.73 \times 10^{11}$
	WGC	34.17	3.28	27.19	$7.59 \times 10^{11}$	$4.19 \times 10^{11}$
	Interior	34.68	4.04	27.53	$1.07 \times 10^{12}$	$1.88 \times 10^{12}$
0–1500	LC	34.38	2.75	27.40	$2.53 \times 10^{12}$	$1.56 \times 10^{12}$
	WGC	34.66	3.59	27.56	$9.10 \times 10^{11}$	$1.35 \times 10^{12}$
	Interior	34.84	3.50	27.71	$2.41 \times 10^{12}$	$7.24 \times 10^{12}$
0–3000	LC	34.48	2.77	27.48	$2.60 \times 10^{12}$	$1.94 \times 10^{12}$
	WGC	34.71	3.46	27.60	$9.48 \times 10^{11}$	$1.56 \times 10^{12}$
	Interior	34.88	3.14	27.77	$3.61 \times 10^{12}$	$12.94 \times 10^{12}$
0–>3000	Interior	34.88	3.00	27.79	$3.91 \times 10^{12}$	$13.68 \times 10^{12}$

TABLE 9. As in Table 4, but for the fall ISO climatology.

Depth range (m)	Region	$S_{mean}$	$\theta_{mean}$ (°C)	$\sigma_{\theta}$	$\Sigma FW$ (m <sup>3</sup> )	$\Sigma H$ (GJ)
0–300	LC	33.43	2.13	26.70	$2.83 \times 10^{12}$	$5.38 \times 10^{11}$
	WGC	34.22	3.77	27.18	$7.09 \times 10^{11}$	$4.79 \times 10^{11}$
	Interior	34.60	4.11	27.46	$1.32 \times 10^{12}$	$1.91 \times 10^{12}$
0–1500	LC	34.25	2.96	27.28	$3.12 \times 10^{12}$	$1.73 \times 10^{12}$
	WGC	34.68	3.84	27.54	$8.53 \times 10^{11}$	$1.43 \times 10^{12}$
	Interior	34.82	3.58	27.68	$2.66 \times 10^{12}$	$7.40 \times 10^{12}$
0–3000	LC	34.38	2.96	27.38	$3.19 \times 10^{12}$	$2.12 \times 10^{12}$
	WGC	34.72	3.67	27.59	$8.93 \times 10^{11}$	$1.63 \times 10^{12}$
	Interior	34.87	3.16	27.76	$3.86 \times 10^{12}$	$13.02 \times 10^{12}$
0–>3000	Interior	34.87	3.07	27.77	$4.07 \times 10^{12}$	$13.41 \times 10^{12}$

details used in creating the product(s), before reporting on the follow-on analysis, especially since no previous, high-resolution isopycnal product for the Labrador Sea exists. These products will be made available to those who may also wish to use them.

### Acknowledgments

We would like to thank Brad deYoung, Len Zedel, Edward Lozowski, Andrew Bush, Bruce Sutherland, Thierry Reynaud

and three anonymous reviewers for their valuable suggestions and discussions and the Bedford Institute of Oceanography for providing the data. This work was funded by the National Sciences and Engineering Research Council (NSERC) and the Canadian Foundation for Climate and Atmospheric Science (CFCAS) (GR-019 and the Canadian CLIVAR Network) grants awarded to PGM. This work is part of the Ph.D. studies of Nilgun Kulan.

TABLE 10. As in Table 4, but for the winter ISO climatology.

Depth range (m)	Region	$S_{mean}$	$\theta_{mean}$ (°C)	$\sigma_{\theta}$	$\Sigma FW$ (m <sup>3</sup> )	$\Sigma H$ (GJ)
0–300	LC	33.46	1.30	26.77	$2.78 \times 10^{12}$	$3.29 \times 10^{11}$
	WGC	34.30	2.44	27.37	$6.27 \times 10^{11}$	$3.08 \times 10^{11}$
	Interior	34.68	3.31	27.60	$1.06 \times 10^{12}$	$1.55 \times 10^{12}$
0–1500	LC	34.23	2.43	27.31	$3.12 \times 10^{12}$	$1.39 \times 10^{12}$
	WGC	34.69	3.35	27.60	$7.63 \times 10^{11}$	$1.16 \times 10^{12}$
	Interior	34.83	3.38	27.71	$2.47 \times 10^{12}$	$6.99 \times 10^{12}$
0–3000	LC	34.37	2.53	27.41	$3.18 \times 10^{12}$	$1.78 \times 10^{12}$
	WGC	34.74	3.27	27.64	$7.98 \times 10^{11}$	$1.38 \times 10^{12}$
	Interior	34.88	3.12	27.78	$3.50 \times 10^{12}$	$12.85 \times 10^{12}$
0–>3000	Interior	34.88	2.99	27.79	$3.77 \times 10^{12}$	$13.58 \times 10^{12}$

## References

- BARNES, S. L. 1964. A technique for maximizing details in numerical weather map analysis. *J. Appl. Meteorol.* **3**: 396–409.
- BÖNING, C. W.; M. RHEIN, J. DENG, and C. DOROW. 2003. Modeling CFC inventories and formation rates of Labrador Sea Water. *Geophys. Res. Lett.* **30** (2), doi: 10.1029/2002GL014855.
- BOYER, T.; S. LEVITUS, H. GARCIA, R. LOCARNINI, C. STEPHENS and J. ANTONOV. 2005. Objective analyses of annual, seasonal, and monthly temperature and salinity for the world ocean on a 1/4 degree grid. *Int. J. Climatol.* **25**: 931–945.
- CLARKE, R. A. 1984. Transport through the Cape Farewell-Flemish Cap section. Int. Council for the Exploration of the Sea, Report 185, pp. 120–130.
- CLARKE, R. A. and J. GASCARD. 1983. The formation of Labrador Sea Water. Part I: Large-scale processes. *J. Phys. Oceanogr.* **13**: 1764–1778.
- CRESSMAN, G. P. 1959. An operational objective analysis scheme. *Mon. Weather Rev.* **87**: 329–340.
- CUNY, J.; P. B. RHINES, P. P. NIILER and S. BACON. 2002. Labrador Sea Boundary currents and the fate of Irminger Sea Water. *J. Phys. Oceanogr.* **32**: 627–647.
- DE YOUNG, B.; F. PERRY and R. GREATBATCH. 1964. Objective analysis of hydrographic data in the northwest Atlantic. Tech. Rep. Can. Data Rep. Hydrogr. Ocean Sci. No. 130, Memorial University of Newfoundland.
- DENGLER, M., J. FISCHER, F. A. SCHOTT and R. ZANTROPP. 2006. Deep Labrador Current and its variability. *Geophys. Res. Lett.* **33**: doi:L21S06/10.1029/1026GL027441.
- DICKSON, R. R.; I. YASHAYAIEV, J. KEINCKE, B. TURRELL, S. DYE and J. HOLFORT. 2002. Rapid freshening of the deep North Atlantic Ocean over the past four decades. *Nature*, **416**: 832–837.
- FISCHER, J.; F. A. SCHOTT and M. DENGLER. 2004. Boundary circulation at the exit of the Labrador Sea. *J. Phys. Oceanogr.* **34**: 1548–1570.
- FLATAU, M. K.; L. TALLEY and P. P. NIILER. 2003. The North Atlantic Oscillation, surface current velocities, and SST changes in the subpolar North Atlantic. *J. Clim.* **16**: 2355–2369.
- GREATBATCH, R. J. and A. GOULDING. 1989. Seasonal variations in a linear barotropic model of the North Pacific driven by the Hellerman and Rosenstein wind stress field. *J. Geophys. Res.* **94**: 12,645–12,665.
- GREGORY, D. N. 2004. Climate: A database of temperature and salinity observations for the northwest Atlantic. Tech. Rep. DFO Can Sci. Advis. Sec. Res. doc. 2004/075, MEDS.
- GREY, S. M.; K. HAINES and A. M. MACDONALD. 1999. Climatological hydrography of the North Atlantic. *Int. WOCE Newsletter*, **36**: 23–25.
- LAVENDER, K. L.; R. E. DAVIS and W. B. OWENS. 2002. Observations of open-ocean deep convection in the Labrador Sea from subsurface floats. *J. Phys. Oceanogr.* **32**: 511–526.
- LAZIER, J. R. N. 1973. The renewal of the Labrador Sea water. *Deep Sea Res.* **20**: 341–353.
- LAZIER, J. R. N. and D. G. WRIGHT. 1993. Annual velocity variations in the Labrador Current. *J. Phys. Oceanogr.* **23**: 659–678.
- LAZIER, J.; R. HENDRY, A. CLARKE, I. YASHAYAIEV and P. RHINES. 2002. Convection and restratification in the Labrador Sea, 1990–2000. *Deep Sea Res.* **49**: 1819–1835.
- LEVITUS, S. 1982. Climatological atlas of the world ocean. Tech. Rep. 13, U.S. Department of Commerce, National Oceanographic and Atmospheric Administration.
- LEVITUS, S. 1994. World Ocean Atlas 1994 CD-ROM sets. Tech. Rep. Informal Report 13, U.S. Department of Commerce, National Oceanographic and Atmospheric Administration.
- LILLY, J. M.; P. B. RHINES, M. VISBECK, R. DAVIS, J. R. N. LAZIER, F. SCHOTT and D. FARMER. 1999. Observing deep convection in the Labrador Sea during winter 1994/95. *J. Phys. Oceanogr.* **29**: 2065–2098.
- LODER, J. W.; B. PETRIE and G. GAWARKIEWICZ. 1998. The coastal ocean off northeastern North America: A large-scale view. In: *The Sea, Volume 11*, A. R. Robinson and K. H. Brink (Eds), John Wiley and Sons, Inc., pp. 105–133.
- LOZIER, M. S.; W. B. OWENS and R. G. CURRY. 1995. The climatology of the North Atlantic. *Prog. Oceanogr.* **36**: 1–44.
- MACDONALD, A. M.; T. SUGA and R. G. CURRY. 2001. An isopycnally averaged North Pacific climatology. *J. Atmos. Ocean. Technol.* **18**: 394–420.
- MYERS, P. G. 2002. SPOM: A regional model of the sub-polar North Atlantic. *ATMOSPHERE-OCEAN*, **40**: 445–463.
- MYERS, P. G.; A. F. FANNING and A. J. WEAVER. 1996. JEBAR, bottom pressure torque and Gulf Stream separation. *J. Phys. Oceanogr.* **26**: 671–683.
- MYERS, R. A.; S. A. AKENHEAD and K. DRINKWATER. 1990. The influence of Hudson Bay runoff and ice-melt on the salinity of the inner Newfoundland shelf. *ATMOSPHERE-OCEAN*, **28**: 241–256.
- NOAA. 1988. Digital relief of the surface of the earth. Tech. Rep. Data Announcement 88-MGG-02. National Geophysical Data Center, Boulder, Colorado.
- PICKART, R. A.; D. J. TORRES and R. A. CLARKE. 2002. Hydrography of the Labrador Sea during active convection. *J. Phys. Oceanogr.* **32**: 428–457.
- RENFREW, I. A.; G. W. K. MOORE, P. S. GUEST and K. BUMKE. 2002. A comparison of surface layer and surface turbulent flux observations over the Labrador Sea with ECMWF analyses and NCEP reanalyses. *J. Phys. Oceanogr.* **32**: 383–400.
- REYNAUD, T. H. 1994. Dynamics of the northwestern Atlantic Ocean. Ph.D. thesis, McGill University.
- REYNAUD, T. H.; A. J. WEAVER and R. J. GREATBATCH. 1995. Summer mean circulation of the northwestern Atlantic Ocean. *J. Geophys. Res.* **100**: 779–816.
- RHEIN, M.; J. FISCHER, W. M. SMETHIE, D. SMYTHE-WRIGHT, R. F. WEISS, C. MERTENS, D.-H. MIN, U. FLEISCHMANN and A. PUTZKA. 2002. Labrador Sea

## Comparing Two Climatologies of the Labrador Sea: Geopotential and Isopycnal / 39

- Water: Pathways, CFC inventory and formation rates. *J. Phys. Oceanogr.* **32**: 648–665.
- SMETHIE, W. M. and J. H. SWIFT. 1989. The tritium:krypton-85 age of Denmark Strait Overflow waters and Gibbs Fracture Zone Water just south of Denmark Strait. *J. Geophys. Res.* **94**: 8265–8275.
- SMITH, S. D. and F. W. DOBSON. 1984. The heat budget at Ocean Weather Station Bravo. *ATMOSPHERE-OCEAN*, **22**: 1–22.
- STEFFAN, E. L. and E. A. D'ASARO. 2002. Deep convection in the Labrador Sea as observed by Lagrangian floats. *J. Phys. Oceanogr.* **32**: 475–492.
- STEPHENS, C.; J. I. ANTONOV, T. P. BOYER, M. E. CONKRIGHT, R. A. LOCARNINI, T. D. O'BRIEN and H. E. GARCIA. 2002. World Ocean Atlas 2001 Volume 1: Temperature. NOAA Atlas NESDIS 49, Washington, D.C.
- STRANEO, F. 2006. Heat and freshwater transport through the central Labrador Sea. *J. Phys. Oceanogr.* **36**: 606–628.
- THOMPSON, K. R.; J. R. N. LAZIER and B. TAYLOR. 1986. Wind-forced changes in Labrador Current transport. *J. Geophys. Res.* **9**: 14,261–14,268.
- THOMPSON, K. R.; D. G. WRIGHT, Y. LU and E. DEMIROV. 2006. A simple method for reducing seasonal bias and drift in eddy resolving ocean models. *Ocean Modelling*, **14**: 122–138.
- YASHAYAEV, I. 2007. Hydrographic changes in the Labrador Sea, 1960–2005. *Prog. Oceanogr.* **73**: 242–276.
- YASHAYAEV, I. M. and I. I. ZVERYAEV. 2001. Climate of the seasonal cycle in the North Pacific and the North Atlantic oceans. *Int. J. Climatol.* **21**: 401–417.
-